PASSIVE DEFENCE STRUCTURES AGAINST DENSE SNOW AVALANCHES EXPERIMENTAL ANALYSIS

OPERE DI DIFESA PASSIVA DA VALANGHE DI NEVE DENSA ANALISI SPERIMENTALE

Paolo Scotton[1], Stefano De Toni[2] and Francesca Moro[3]

ABSTRACT

The article presents an experimental investigation performed at the Hydraulic Laboratory of the University of Trent in order to analyse the behaviour of some passive defence structures used in the practice of environmental engineering in order to slow down dense snow avalanches. The research considers retarding mounds and teeth, taken as single elements and in a system of three elements arranged in two lines. The article describes the experimental set-up, that can simulate the real phenomena following the Froude similarity with a geometrical scale of about 1:100, and gives some criteria for the estimation of the impact force against front and rear works . It is described the most efficient works layout and it is shown that maximum efficiency occurs when maximum dimensionless force occurs.

Keywords: passive defence structures, dense snow avalanches, granular flows.

RIASSUNTO

L'articolo presenta una indagine sperimentale realizzata presso il Laboratorio di Idraulica dell'Università di Trento al fine di analizzare il comportamento di alcune opere di difesa passiva utilizzate nella pratica professionale per rallentare le valanghe di neve densa. Vengono presi in considerazione i coni e i denti frenanti, come elementi singoli e in un sistema di tre opere disposte su due file. L'articolo descrive l'apparato sperimentale, che può simulare i fenomeni reali in similitudine di Froude in scala geometrica di circa 1:100 e fornisce dei criteri per la stima della forza di impatto e per la valutazione dell'efficienza dei sistemi di opere considerati nel ridurre la distanza di arresto e nel produrre maggiore dispersione laterale della massa.

Keywords: strutture di difesa passiva, valanghe di neve densa, flussi granulari.

1 Ass. Prof., Department of Geosciences, University of Padua, Via Giotto 1, 35137 Padova, ITALY (tel: +39-049-827-1865; fax: +39-049-827-2070; e-mail: paolo.scotton@unipd.it).
2 PhD, Department of Civil and Environmental Engineering, University of Trento, Via Mesiano 77, 38100 Povo (TN), ITALY (Tel.: +39-0461-882603; Fax: +39-0461-882672; email: stefano.detoni@ing.unitn.it).
3 PhD student, Department of Geosciences, University of Padova, Via Giotto 1, 35137 Padova, ITALY (tel: +39-049-827-2050; fax: +39-049-827-2070; e-mail: francesca.moro@unipd.it).

INTRODUCTION

In Alpine regions snow avalanches are a severe threat for human settlements, activities, infrastructures. The only countermeasure against powder snow avalanches is to prevent the initiation of the motion by means of active structures, built in the detachment area, or to trigger artificially avalanches events. Besides, passive structures along the path and in the run-out zone can be very effective in deviating, retarding or stopping dense snow avalanches (e. g. Faug et alii, 2004; Johannesson et alli, 2006). In order to deep some aspects of the behaviour of some types of structures against granular avalanches, an experimental campaign has been carried out at the Hydraulic Laboratory of the Faculty of Engineering of the University of Trento.

EXPERIMENTAL APPARATUS

The flume and its support

The experiments have been performed using the experimental support showed in Fig. 1. It is formed by two tiltable planes made of Forex, squared shaped, whose lateral dimension is 150 cm. The upper plane can be tilted from 0° to 35°, while the lower plane can be tilted from 0° to roughly 10°. Connection between upper and lower plane has been made by an elastic strip. On the upper plane has been realized a channel whose lateral walls are made of transparent Perspex. The width of the flume is 20 cm and the height of the lateral walls is 15 cm. The flume ends about 20 cm upstream the change of slope. In the very upper part of the flume has been realized a feeding box where the granular material was placed before the execution of the experiments. The slowing down works have been located in the upper plane downstream the flume. After the impact against the retarding works, the granular material used to simulate a dense snow avalanche can freely spread in the on the lower plane.

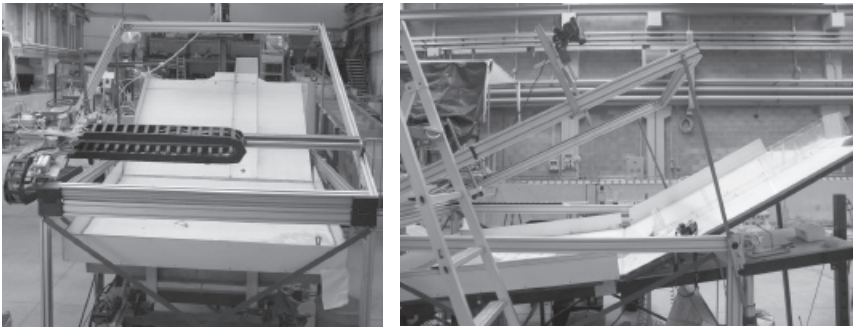

Fig1: On the left, a view of the flume and of its support structure; on the right a lateral view of the experimental apparatus.
Fig1: Sulla sinistra una vista da valle della canaletta e della struttura di supporto; sulla destra una vista laterale dell'apparato sperimentale.

The feeding box

The feeding box (Fig. 2) has been obtained by means of a removable vertical gate made of Forex. The gate has been fitted into two small grooves obtained in the lateral walls. The cross section of the box is the same of the flume. Its length is about 30 cm. The box volume is roughly 9 litres.

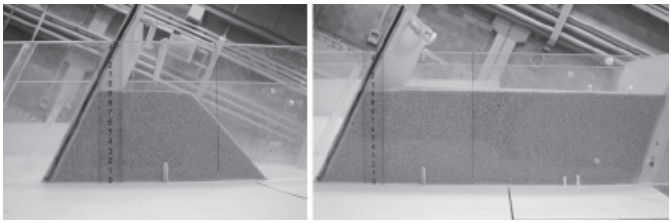

Fig2: The feeding box, at the superior extreme of the flume, and the mixture arrangement of 29 N (3 kg), on the left, and of 69 N (7 kg).
Fig2: Il serbatoio di carico all'estremo superiore della canaletta di prova. Sulla sinistra la disposizione di tre kg del materiale granulare; sulla destra la disposizione di 7 kg.

The granular material

The granular material (Fig. 3) used in the experiments is made by zeolite, a synthetic resin. The shape of the grains is roughly spherical. The diameters range from 0.1 mm to 2 mm, with a mean diameter of about 1 mm. The specific weight of the resin is 1080 kg/m^3.

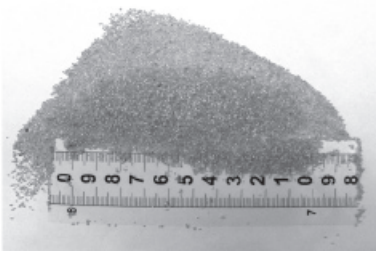

Fig3: The granular material, obtained from zeolite, a synthetic resin, used to form the flowing mass.
Fig3: Il materiale granulare, ottenuto dalla zeolite, una resina sintetica, utilizzato nelle prove sperimentali.

The retarding mounds and walls

Various types of slowing down elements (Fig. 4) have been used to simulate the shape of works actually designed in the field. A first series of tests have been conducted using wooden made cones, with a height of 30 mm and base diameter of 30 mm, and vertical elements (teeth), equally wooden made, with a height of 30 mm and width of 44 mm. In a following series of tests three cone-derived elements have also been tested. They have been realized taking into account that real works present an angle on the horizontal of the upstream face of about 40°. Nylon has been the used material. Their height has been 30 mm, the shape

depended on the slope of upstream plane. The weight of the elements was ranging from 20 g to 30 g (in order to reduce, as much as possible, inertial effects). To this goal the nylon elements have been lightened scouring the inner volume.

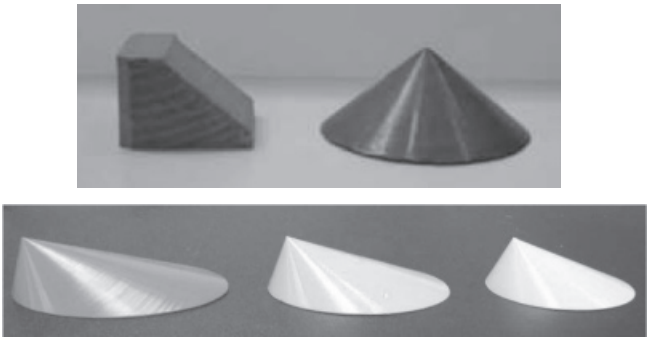

Fig4: The retardingelements used in the experiments. Above on the left, the tooth (vertical wall); above on the right, the circular base cone; below three elliptical base cones used, respectively, at the inclinations of 30°, 27° and 24°.
Fig4: Gli elementi rallentatori utilizzati negli esperimenti. Sopra, sulla sinistra, il dente; sulla destra, il cono a base circolare. Sotto, tre coni a base ellittica usati, rispettivamente, a 30°, 27° e 24° di inclinazione sull'orizzontale della canaletta sperimentale.

The support of the slowing down elements

The single slowing down element (cone or tooth) is connected with a T-support (Fig. 5) which is a linear low-friction sliding mechanism. The force experienced by the element is transmitted to the load cell mounted onto the T-support. No moment is transmitted. All the slowing down elements (three at the maximum) are mounted onto a support plate which is placed underneath the upper plane.

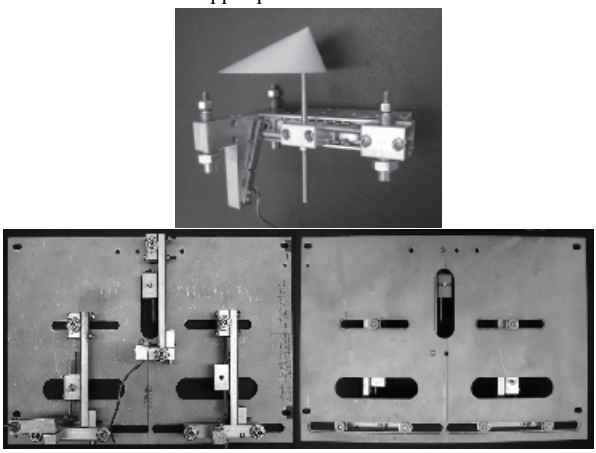

Fig5: Above, the T-support used to transfer the force acting on the slowing down element; below, a view from below, on the left, and from above of the support plate of the T-supports. The plate is mounted underneath the flume support.

Fig5: Sopra, il supporto a T usato per la trasmissione della forza agente sull'elemento rallentatore; sotto, sulla sinistra, una vista dal basso e, sulla destra, dall'alto della piastra di supporto dei supporti a T. La piastra è montata al di sotto della struttura di supporto della canaletta.

The load cells

Two types of load cells have been used to perform the laboratory experiments (Fig. 6): Futek model L1510 (protected) and Futek model L1501 (not protected). After a series of preliminary tests two capacities have been chosen: 1 lb (4.5 N) and 2 lb (8.9 N). The sensitivity of the 1 lb model is 0.002 lb (0.906 g), while the sensitivity of the 2 lb model is 0.0004 lb (0.181 g). The response time of both types of the load cells has been assessed experimentally lower than 0.005 s.

Fig6: The load cells used in the experiments to measure the force against the retarding elements. On the left, the non-protected model; on the right, the protected model.
Fig6: Le celle di carico utilizzate negli esperimenti per la misura della forza di impatto sugli elementi rallentatori. Sulla sinistra il modello non protetto, sulla destra il modello protetto.

The measurement of flow velocity and height

The measurement of flow velocity (Fig. 7) and height (Fig. 8) have been obtained by means of two video-cameras. One digital video-camera has been located above the upper plane in order to cover the area between the end of the flume and the slowing down elements. The second digital video-camera was located laterally to the final part of the flume in order to shoot the flowing height of the mixture at a section very near to the works.

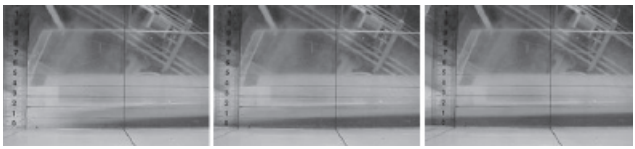

Fig7: A sequence of frames obtained by the lateral video-camera. The image processing allows to estimate the height of the flowing mixture near to the retardingelements.
Fig7: Una sequenza di immagini ottenute dalla video-camera posta lateralmente alla canaletta. La analisi delle immagini permette di stimare la altezza di scorrimento della mistura in prossimità degli elementi rallentatori.

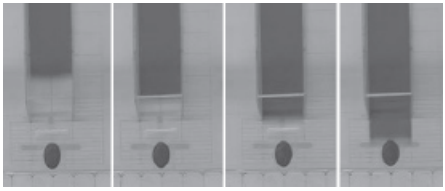

Fig8: A sequence of frames obtained by the frontal video-camera. The image processing allows to estimate the velocity of the flowing mixture near to the retarding elements.
Fig8: Una sequenza di immagini ottenute dalla video-camera frontale. La analisi delle immagini permette di stimare la velocità di scorrimento del fronte della mistura in prossimità degli elementi rallentatori.

The measurement of mixture spreading

The measurement of final longitudinal and cross-sectional mixture spreading has been obtained by image processing of pictures of the type of Fig. 9. Mixture spreading depends on type of works (circular base cones, elliptical base cones and teeth) and on the respective position of the elements. The rear line of works is located at a longitudinal distance from the upstream element of about twice the height of the works (70 mm). The rear elements can be located at various positions along the cross-sectional guide. The angle θ, between the longitudinal flow direction and the line passing through the front and the rear element (see Fig. 10), ranges from 25° to 50°.
Two physical parameters have been defined in order to characterize the mixture spreading: the longitudinal efficiency and the cross-sectional efficiency (Fig. 11).
The cross-sectional efficiency is defined as follows:

$$\varepsilon_T = \frac{L - L_{NW}}{L_{NW}},$$

where L is defined as in Fig. 11 and L_{NW} is the maximum width of the mixture at rest in the case of absence of slowing down elements.
The longitudinal efficiency is defined as follows:

$$\varepsilon_L = \frac{d_{NW} - d}{d_{NW}},$$

where d is defined as in Fig. 11 and d_{NW} is the maximum distance travelled by the mixture in the case of absence of slowing down elements.

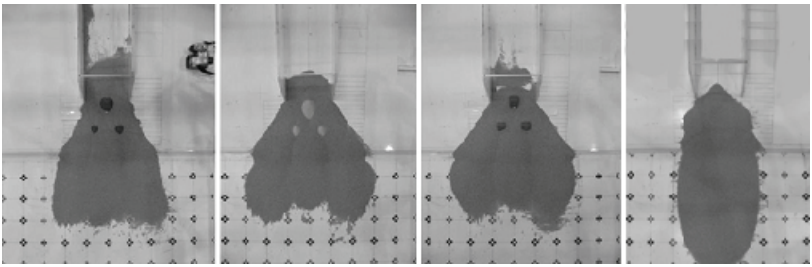

Fig9: Three examples of mass spreading caused by a particular layout of three circular base cones, on the left, three elliptical base cones and three teeth (vertical walls). On the right the mass spreading without retarding works.
Fig9: Tre esempi di dispersione della mistura fluente causati da una particolare disposizione di tre coni a base circolare, sulla sinistra, di tre coni a base ellittica e di tre denti. Sulla destra un esempio senza opere.

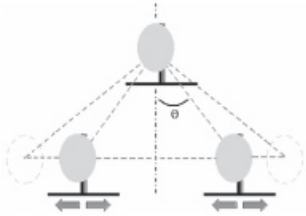

Fig10: Scheme of elements layout. The rear works forms an angle θ with the longitudinal flow direction.
Fig10: Schema distributivo degli elementi rallentatori. Le opere posteriori formano un angolo θ con la direzione longitudinale del flusso.

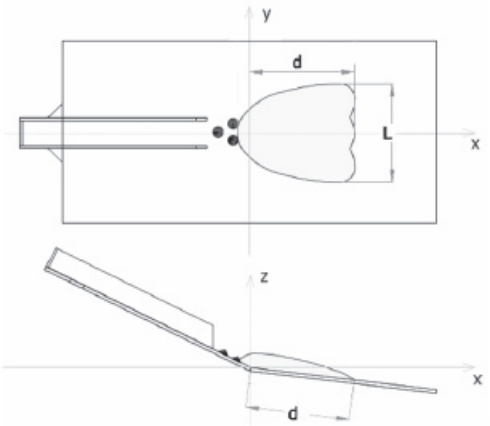

Fig11: Scheme showing the physical parameters used to define the longitudinal and the cross-sectional efficiency of the retardingelements.
Fig11: Schema che illustra i parametri fisici utilizzati per la definizione dell'efficienza longitudinale e trasversale degli elementi rallentatori.

EXPERIMENTS

About 130 runs have been analysed for the present paper. The lower plane inclination has been held at 7° (an inclination that is of the same order of magnitude of natural stopping zone inclination). The upper plane inclinations were 24°, 27° and 30° (three values in the range of variation of flowing zone inclinations). Two material weights have been chosen: 29,43 N (3 kg) and 68,67 (7 kg). Five rear works opening angle have been chosen: 26°, 30°, 35°, 40° and 45°. Some experiments have been performed without any slowing down element in order to be able to assess the efficiency of the system. Many experimental configuration have been performed twice or three times with the goal to verify their repeatability.
The calibration of the force measurement system has been done (see Fig. 12) before the execution of each test. Particular attention has been placed in order to avoid that some grains of the mixture could get stuck between the base of the slowing down elements and the support plane and in the mechanical system underneath the plane, giving serious problems in the measurement of impact force.

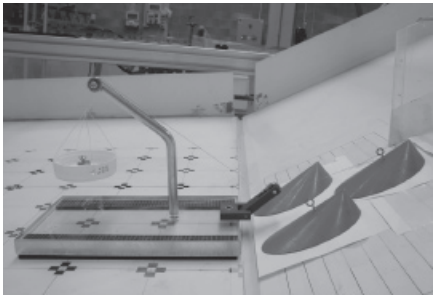

Fig12: The experimental set-up used to perform the on site calibration of the force measurement system.
Fig12: L'apparato sperimentale utilizzato per la calibrazione del sistema di misura della forza di impatto.

SOME EXPERIMENTAL RESULTS

The physical parameters that have to be considered important for the present phenomenon are the impact force (F), the height of the mixture (h: the maximum value at the final section of the flume), the velocity of the mixture (v) near to the works, the shape and dimension of the slowing down works (circular base cone, elliptical base cone, tooth), the geometrical distribution of the retarding elements, the shape of the deposit, the maximum width of the deposit (L), the maximum longitudinal distance reached by the deposit (d), the bulk density of the mixture in the area of the impact, the cross sectional dimension of the flow. The volume of the mixture and its shape at the beginning of the motion, the rheology of the mixture, the slope of the flume and its bottom and side walls roughness contribute to define all the properties of the mixture distribution before the impact.
As written above, not all the cited parameters have been investigated. In particular it was not possible to define the bulk density of the mixture. For this reason in the presentation of the experimental results the density of the material has been used. Some particular shapes of retarding elements have been investigated, in order to simulate geometrically the types of works that are used in the real cases. Also the distribution of the retarding elements tend to simulate the disposition adopted in real designs limited to two elements lines. The ratio between the width of the flowing mass and the width of the retarding elements is always the same and not far from the unity.
In the experiments the measured values of the mixture height ranged from 8 mm to 21mm; the values of velocity from 1.5 m/s to 2.6 m/s; the Froude number ranged from 4 to 8.; the values of force against the front element from 0.64 N to 2.84 N, while against the rear elements from 0.16 N to 2.26 N. About 20 tests have been performed in order to examine repeatability. The mean variability of dimensionless force (see below) was of about 12 %, with a standard deviation of about 10 %.

The dimensionless force – front element

Dimensionless impact force has been obtained by means of the material density (the density of zeolite $\rho = 1080$ Kg/m^3), the velocity of the mixture flow near to the works (v) and the impact area (A):

$$F_{d\_less} = \frac{F}{\rho v^2 A}.$$

The impact area is defined as in Fig. 13.

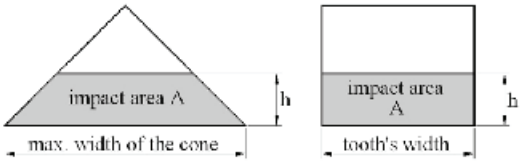

Fig13: Definition of impact area for the cones and for the teeth used in the evaluation of dimensionless impact force.
Fig13: Definizione dell'area di impatto nel caso dei coni e dei denti usata nella valutazione della forza di impatto adimensionale.

In Fig. 14, Fig. 15 and Fig. 16 dimensionless impact force is showed for circular base cones, elliptical base cones and teeth. The behaviour of the two types of cones doesn't differ significantly.

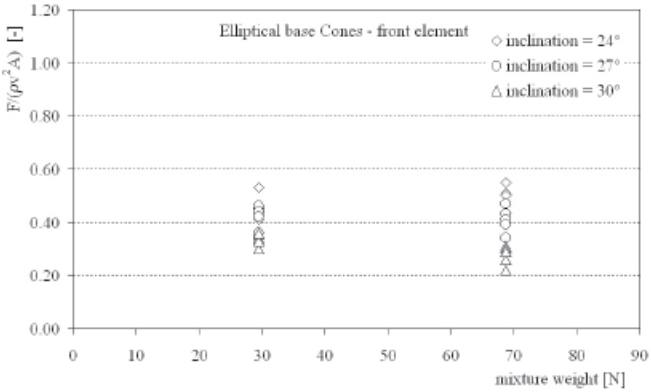

Fig14: Dimensionless impact force against retarding elements having the shape of elliptical base cones at various inclination angles and at various mixture weight.
Fig14: Forza adimensionale di impatto sugli elementi conici a base ellittica al variare della pendenza della canaletta e dell'angolo di apertura degli elementi rallentatori.

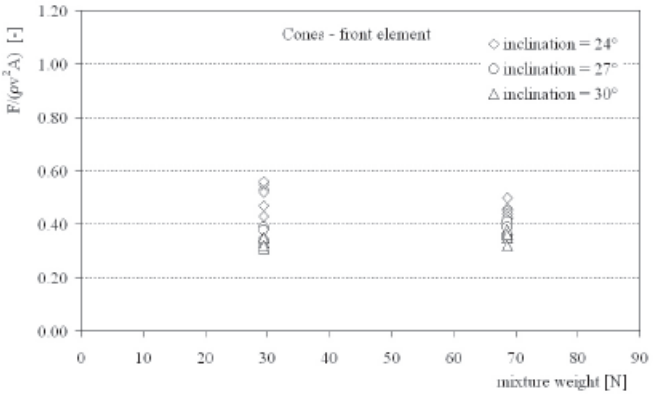

Fig15: Dimensionless impact force against retarding elements having the shape of circular base cones at various inclination angles and at various mixture weight.

Fig15: Forza adimensionale di impatto sugli elementi conici a base circolare al variare della pendenza della canaletta e dell'angolo di apertura degli elementi rallentatori.

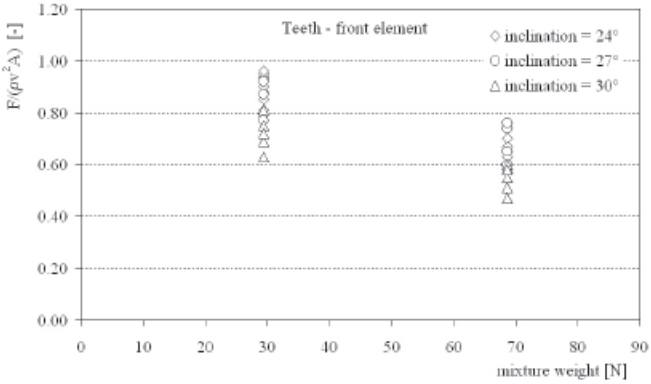

Fig16: Dimensionless impact force against retardingelements having the shape of vertical walls at various inclination angles and at various mixture weight.
Fig16: Forza adimensionale di impatto sui denti al variare della pendenza della canaletta e dell'angolo di apertura degli elementi rallentatori.

The mean value of

F_{d_less} is 0.41 for circular base cones, while is 0.40 for elliptical base cones. A certain variability, observable around the mean value, should be mostly due to the variability of the bulk density, the parameter that should be more correctly used to construct the dimensionless force.
In case of vertical wall retarding elements the mean value of the dimensionless force is much greater and equal to 0.74. In this case, besides the dispersion around the mean value, it is observable a different mean value in the tests performed with a weight of material of 29 N and the tests with a weight of 69 N. For this behaviour should be responsible another important dimensionless parameter: the relative height, defined as the ratio between the height of the flowing mixture and the height of the retarding elements. The dimensionless impact force is bigger when the relative height is lower.

The dimensionless force – rear elements

In Fig. 17, Fig. 18 and Fig. 19, dimensionless impact force is showed for the three types of considered retarding elements located in the rear line, when the opening angle changes from 25° to 45°. Velocity v and impact area A are the same used for the front element.

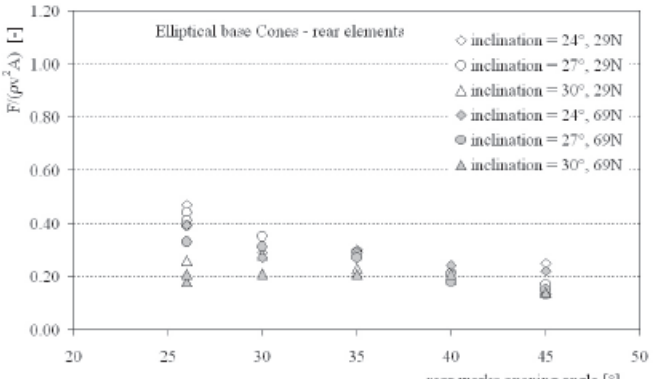

Fig17: Dimensionless impact force against rear retardingelements having the shape of elliptical base cones at various inclination angles, at various mixture weight and at various opening angles.

Fig17: Forza di impatto adimensionale sui coni a base ellittica della fila posteriore al variare della pendenza della canaletta e dell'angolo di apertura delle opere.

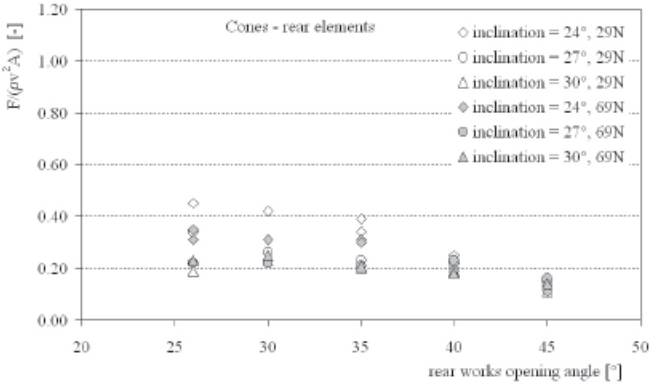

Fig18: Dimensionless impact force against rear retardingelements having the shape of circular base cones at various inclination angles, at various mixture weight and at various opening angles.

Fig18: Forza di impatto adim. sui coni a base circolare della fila posteriore al variare della pendenza della canaletta e dell'angolo di apertura delle opere.

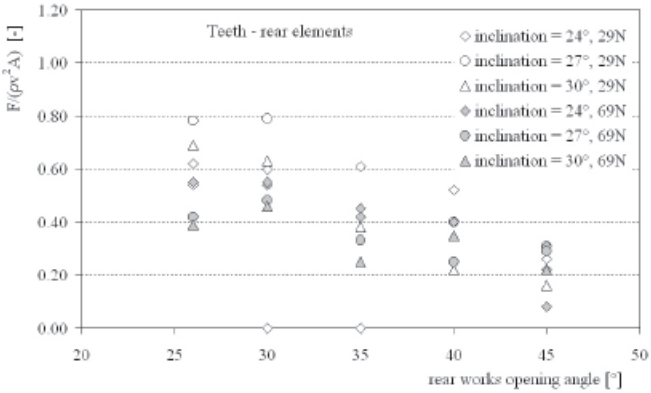

Fig19: Dimensionless impact force against rear retardingelements having the shape of vertical walls at various inclination angles, at various mixture weight and at various opening angles.

Fig19: Forza di impatto adimensionale sui denti della fila posteriore al variare della pendenza della canaletta e dell'angolo di apertura delle opere.

In the Fig. 20 the mean value of dimensionless impact force is showed. At the rear position, in case of cones, the maximum impact force is produced with an opening angle which is less than 26°. On the other hand, in case of vertical wall elements the maximum impact force was observed at opening angles near to 30°.

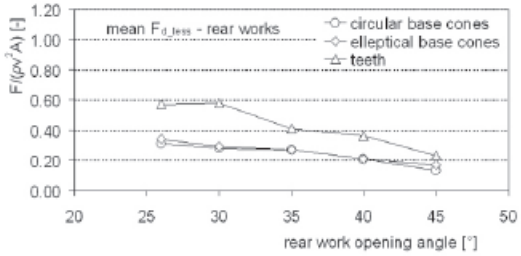

Fig20: Behaviour of the mean value of dimensionless impact force for the rear retardingelements when the opening angle varies from 25° to 45°.

Fig20: Andamento del valore medio della forza di impatto adimensionale per le opere della fila posteriore al variare dell'angolo di apertura.

Longitudinal and cross-sectional efficiency

In Fig. 21 and Fig. 22 the efficiency of the systems are plotted when the opening angle of rear works varies from 25° to 45°. All the retarding systems tend to reduce their longitudinal and cross-sectional efficiency when the opening angle is larger than 25°. Around 25°-30° the efficiency of teeth and elliptical base cones appears to be larger than the efficiency of circular base cones. Nevertheless, as the opening angle increases, it is visible a more regular behaviour of the efficiency loss when using cones. The maximum longitudinal and cross-sectional efficiency tends to occur when the maximum dimensionless force occurs.

CONCLUSIONS

The paper gives some technical information that can be used in the designing process of retarding works against dense snow avalanches. It provides some criteria to estimate the maximum total force acting on different types of structures, once the main physical parameters that characterize the flowing mass are defined, for instance by a numerical dynamic analysis. It shows that dimensionless force is much bigger for the systems that use

vertical wall elements instead of cone shaped structures, that the opening angle of the rear structures at which the cross-sectional and the longitudinal efficiency present their maximum value is less than 26° and that the maximum efficiency happens when the dimensionless force is the maximum

The phenomena produced in the laboratory can be thought to represent real phenomena in the Froude similarity at a scale of the order of magnitude of roughly 1:100. A confirmation of the experimental results should be given at a higher scale.

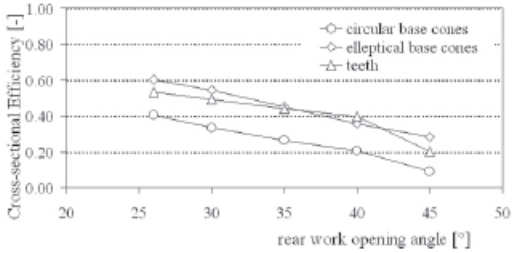

Fig21: Behaviour of the mean value of the cross-sectional efficiency of the retarding system when the opening angle varies from 25° to 45°.

Fig21: Andamento del valore medio dell'efficienza trasversale del sistema di rallentamento al variare dell'angolo di apertura delle opere posteriori.

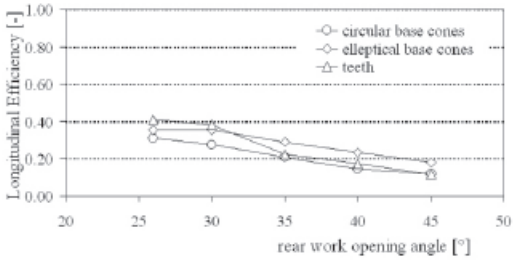

Fig22: Behaviour of the mean value of the longitudinal efficiency of the retarding system when the opening angle varies from 25° to 45°.

Fig22: Andamento del valore medio dell'efficienza longitudinale del sistema di rallentamento al variare dell'angolo di apertura delle opere posteriori.

REFERENCES

Johannesson, T., alii, 2006, The design of avalanche protection dams. Recent practical and theoretical developments (www.leeds.ac.uk/satsie/).

Faug, T., Naaim, M., Naaim-Bouvet, F., 2004, An equation for spreading length, center of mass and maximum run-outs shortenings of avalanche flows by obstacle, Cold Regions Science and Technology 39, 141-151.

ACKNOLEDGMENTS

The authors would like to thank Ilaria Bezzi and Patrizia Pederzolli, involved in the research during their degree thesis. Besides they need to thank all the technicians of the Laboratory of Hydraulics of the University of Trento.